Mesoscopic g-factor renormalization for electrons in III-V interacting nanolayers

M. A. Toloza Sandoval, J. E. Leon Padilla and A. Ferreira da Silva
Instituto de Física, Universidade Federal da Bahia, 40210-340, Salvador, Bahia, Brazil

E. A. de Andrada e Silva
Instituto Nacional de Pesquisas Espaciais, 12201-970, São José dos Campos, São Paulo, Brazil

G. C. La Rocca
Scuola Normale Superiore and CNISM, Piazza dei Cavalieri 7, I-56126, Pisa, Italy

The physics of the renormalization of the effective electron g-factor by the confining potential in semiconductor nanostructures is theoretically investigated. The effective g factor for electrons in structures with interacting nanolayers, or coupled quantum wells (QWs), is obtained with an analytical and yet accurate multiband envelope-function solution, based on the linear 8x8 kp Kane model for the bulk band structure. Both longitudinal and transverse applied magnetic fields are considered and the g-factor anisotropy (i.e. the difference between the two field configurations) analyzed over the entire space spanned by the two structure parameters: the thickness of the active layers and the thickness of the tunneling barrier separating them. 2D anisotropy maps are constructed for symmetric and asymmetric $InGaAs$ coupled-QWs, with InP tunneling barriers, that reproduce exactly known single layer or QW results, in different limits. The effects of the structure inversion asymmetry (SIA) on the mesoscopic g-factor renormalization are also discussed, in particular the negative anisotropies for thin layer structures. Such multi-layer structures form an excellent testing ground for the theory and the analytical solution presented, which is perfectly consistent over the whole space of parameters, leads to helpful expressions and can guide further research on the mechanisms of this mesoscopic renormalization.

Simple GaAs/AlGaAs quantum wells (QWs) represent the ultimate testing system for quantum confinement effects and fundamental methods in condensed matter physics. For instance, the energy quantization and the validity of the envelope-function approximation have been verified in these nanostructures with great accuracy and interest [1]. Semiconductor QWs support 2DEGs and are applied in a large number of electronic devices, in particular lasers and photo-detectors, with operation frequencies tuned by the well width L_w [2]. More recently, high quality structures with tunnel-coupled QWs have been fabricated and used in problems and applications in the physics of exciton liquids [3], topological transitions [4] and special field-effect transistors [5], for example. Considering the 1D dynamics along the growth axis, a double quantum well (DQW) behaves with respect to the constituent QWs similarly to a biatomic molecule with respect to the atoms. These DQW structures support interacting 2DEGs and allow for tunnelling effects used for instance to control the charge transfer between the active layers. With respect to single QWs, DQWs form more general quantum structures with at least two independent parameters: L_w and L_b, the active layer width and that of the barrier in between, which is the inverse of the tunnel-coupling parameter. The single QW limit of the DQW structures, both when $L_b = 0$ and when it is sufficiently large (so that the inter-well coupling is negligible), is a condition of particular interest in the modeling of fine quantum confinement effects, as the g-factor renormalization and the corresponding Zeeman splitting in such nanostructures.

Due to the increasing interest in spintronics [6] and in new schemes for quantum computation, including the detection of Majorana fermions [7], much attention has been given to the renormalization of the electron g factor in semiconductor nanostructures [8–18]. The mesoscopic confining potential in semiconductor nanostructures further renormalizes the bulk effective g factor (already renormalized from the bare value 2) and introduces extra anisotropies, transforming scalar g factors into tensors. The g-factor engineering starts to be a fundamental part of semiconductor physics [19], however it is still largely based only on the Roth formula for the bulk [20] and before achieving the desired control in nanostructures (quantum wells, wires etc), the problems found when modeling and measuring this mesoscopic renormalization in simple III-V QWs need to be solved.

After the work of many groups [21–39], it is by now well established that the ground-state effective g factor for electrons confined in regular GaAs-like QWs (g^{QW}) varies with L_w interpolating from the bulk barrier (AlGaAs) to the bulk well (GaAs) g factors, when L_w goes from zero to a sufficiently large value; and that between these two bulk limits, $g^{QW}(L_w)$ depends on the magnetic-field orientation. The difference in the QW g factor between the magnetic-field orientations perpendicular and parallel to the interfaces, gives the g-factor main anisotropy Δg^{QW} $(= g_{\|} - g_{\perp})$ which is the most direct and critical signature of the quantum confinement, and has been much investigated both theoretically [13, 14, 17, 22, 40] and experimentally [8, 24, 26, 32, 38]. QW structures made out of different compounds were investigated and it is known for example that, except for very thin asymmetric wells [13], electrons in GaAs-

like QWs have larger in-plane g factors ($g_\parallel$) and Δg^{QW} positive. The L_w dependence of the anisotropy is more interesting. In symmetric QWs, the anisotropy must satisfy strict bulk limits, that impose $\Delta g^{QW}(L_w = 0)$ and $\Delta g^{QW}(L_w \to \infty)$ both exactly zero, and present a critical L_w with maximum (or minimum) Δg^{QW}. However it has not been easy to observe and verify these properties. Experimentally, special conditions for the electron spin resonance [24] or sophisticated time-resolved techniques [26, 32] have been necessary and, nevertheless, Δg^{QW} has been measured only with large uncertainties and a small number of samples.

From the theoretical point of view, despite the need of corrections due to the remote bands, the envelope-function approximation based on the 8-band Kane model remains the most promising approach, in particular to obtain general results and expressions, with simple physical interpretations. However, with this same approach, there are different approximate solutions for the effective g factor [22, 24, 31, 40]. The simple analytical solution proposed in Ref. [40] (see also Ref. [13] for details) has the advantages of satisfying exactly the above mentioned bulk conditions in Δg^{QW} and of leading to useful expressions, but has been applied only to single layers or QWs. The extension and application of such solution to more complex and general structures, including for example competing inversion asymmetry (SIA) and tunneling effects, is a critical test of the theory and a clear step forward in our understanding of the mesoscopic g-factor renormalization.

This is what we do here: a detailed and complete solution for the electron effective g factor in symmetric and asymmetric III-V interacting layers or DQW structures. The obtained results are perfectly coherent over the entire space of the structure parameters, exactly reproduce known single QW results in the two corresponding limits, and include helpful expressions and recipes for the estimation/calculation of the effective g-factor in general III-V nanostructures. The interacting features observed between the non-interacting (single QW) limits, as well as the effects of SIA, are simply explained in terms of the Rashba spin-orbit coupling and the electron wave-function in these structures. As a specific example, 2D anisotropy maps $\Delta g^{DQW}(L_w, L_b)$ are constructed for symmetric InP/InGaAs/InP/InGaAs/InP and asymmetric Insulator/InGaAs/InP/InGaAs/InP multi-layer structures, and discussed in detail. Next we present and discuss the model calculation and then the results, before giving a summary of the main conclusions.

A general anisotropic Zeeman response to an applied magnetic field $\vec{B}$ is described by an effective g-factor tensor g^*_{ij} defined by the following Zeeman term in the electron effective Hamiltonian:

$$\mathcal{H}^*_Z = \frac{\mu_0}{2}\,\sigma_i\, g^*_{ij} B_j, \tag{1}$$

with $i, j = x, y, z$, $\vec{\sigma} = (\sigma_x, \sigma_y, \sigma_z)$ being the Pauli matrices spin-vector, and $\mu_0 = e\hbar/2m_0$ the Bohr magneton, with e and m_0, the free electron charge and mass. In 2D structures (QWs, DQWs etc), of the nine independent elements of g^* only two are non zero in first order: $g_\parallel$ and $g_\perp$, diagonal elements corresponding to magnetic fields parallel and perpendicular to the interfaces. In this approximation we neglect the much smaller off-diagonal elements, which include the in-plane anisotropy.

Starting with the applied magnetic field $\vec{B}$ parallel to the interfaces (say in the y-direction, with the growth direction along z), the following effective Hamiltonian for electrons in 2D structures can be easily derived from the linear 8×8 Kane model [40]:

$$\begin{aligned}\mathcal{H}^*(z,\varepsilon) = &-\frac{\hbar^2}{2}\frac{d}{dz}\frac{1}{m(z,\varepsilon)}\frac{d}{dz} + \frac{1}{2}\frac{m_0^2}{m(z,\varepsilon)}\omega_c^2\,(z-z_c)^2 \\ &+E_c(z) + \frac{\mu_0}{2}\sigma_y\left\{g_0 - \frac{4\,m_0}{\hbar^2}\left[\beta(z,\varepsilon) + (z-z_c)\,\frac{d}{dz}\beta(z,\varepsilon)\right] + \delta g_{rem}(z)\right\}B\,.\end{aligned} \tag{2}$$

All different terms above are easily recognized, the last one being the effective Zeeman interaction; g_0 (= 2) being the bare electron g factor, $\omega_c = eB/m_0$ the cyclotron frequency, $\beta(z,\varepsilon)$ the spin-orbit coefficient, $\frac{d}{dz}\beta = \alpha_R$ the so-called Rashba coupling parameter [41–43], $\delta g_{rem}(z)$ the remote bands correction and $z_c = -\ell^2 k_x$ the center of the cyclotron orbit with magnetic length $\ell = \sqrt{\hbar/eB}$ (note that the Hamiltonian does not depend on x, so that a plane wave was chosen for the x-depend part of the wave-function). In addition, $E_c(z)$ describes the conduction-band-edge profile, and for completeness, we recall that the energy-dependent effective mass and spin-orbit coefficient are given by

$$\frac{1}{m(z,\varepsilon)} = \frac{P^2}{\hbar^2}\left[\frac{2}{\varepsilon - E_v(z)} + \frac{1}{\varepsilon - E_v(z) + \Delta(z)}\right] \tag{3}$$

and

$$\beta(z,\varepsilon) = \frac{P^2}{2}\left[\frac{1}{\varepsilon - E_v(z)} - \frac{1}{\varepsilon - E_v(z) + \Delta(z)}\right], \tag{4}$$

where P is the Kane matrix element, $E_v(z)$ (= $E_c(z)$ –

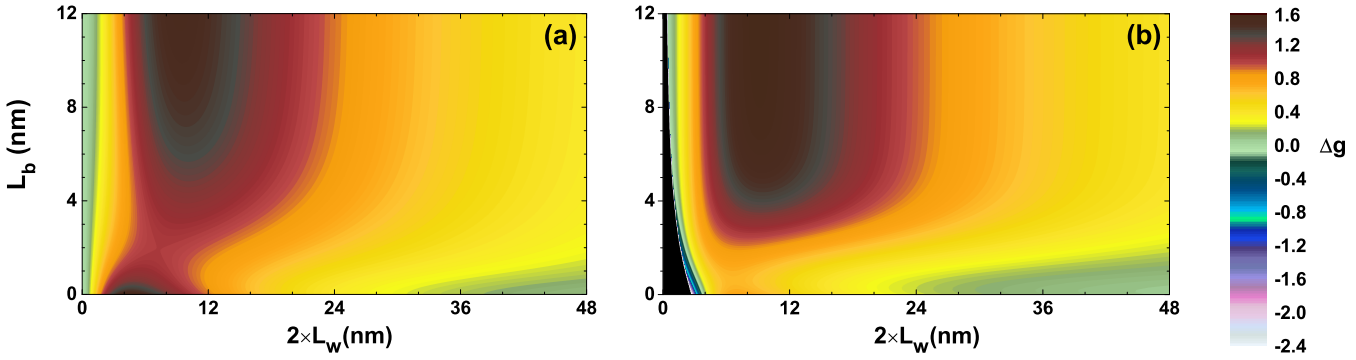

FIG. 1. (Color online) 2D maps of the g-factor anisotropy for electrons in symmetric (a) and asymmetric (b) InGaAs/InP DQW structures. The anisotropy is given by the color code on the right. Among other features discussed in the text, note the large negative values of the anisotropy in asymmetric structures with very thin layers, in the lower left angle of the map, right next to the black area on the left, which is the region with no bound states allowed. For the band profile and parameters, please see Figures 2 and 3.

$E_g(z)$) stands for the valence-band edge profile and Δ is the valence-band spin-orbit energy splitting.

It is easy to check that the above effective Hamiltonian (2) satisfies exactly three well known and fundamental limits: bulk (no z-dependence), no spin-orbit ($\beta = 0$) and zero-field ($B = 0$). More important here though is that in the limit of $B \to 0$, $g_\parallel$ can be obtained in first order perturbation theory. One simply compute the expectation value $\langle \mathcal{H}_Z^* \rangle_{\psi_0}$ with the unperturbed eigenstate ψ_0 (with energy ε_0). The unperturbed problem is that for $B = 0$, i.e. $\mathcal{H}^*(B=0)|\psi_0\rangle = \varepsilon_0|\psi_0\rangle$. By recalling that in an undoped (flat-band) structure $\beta(z)$ is given by a step function, with discontinuous jumps at each interface (where it changes from one bulk value to another), one clearly sees that $g_\parallel = \langle g_{bulk} \rangle_{\psi_0} + \Delta g^{2D}$, i.e. sum of the bulk average plus an interface contribution [40]

$$\Delta g^{2D} = (4\, m_0/\hbar^2) \langle \alpha_R(z, \varepsilon_0)\, (z_0 - z) \rangle_{\psi_0}, \qquad (5)$$

where $z_0 = \langle z \rangle_{\psi_0}$. Even for 2D structures with band profiles far from flat, there is always the $\alpha_R \neq 0$ contribution at the interfaces, which is proportional to $\delta\beta = \beta_w - \beta_b$, the only one for flat-bands and often the dominant one. Since the bulk average is independent of the field and/or growth orientation, Δg^{2D} is identified as the g-factor anisotropy because, in the same order of approximation, one finds $g_\perp = \langle g_{bulk} \rangle_{\psi_0}$. Despite the larger symmetry, the theory for the perpendicular configuration is less straightforward [13, 31], nevertheless, the result could not be simpler, more reasonable and in better agreement with the experiments [23, 25, 26, 32, 36]. In a more usual form, the averaged g_{bulk} can be written in terms of the main parameters as:

$$g_\perp = g_0 - \sum_{i=b,w} \left(\frac{m_0}{m_i(\varepsilon_0)} \frac{2\Delta^{(i)}}{3\varepsilon_g^{(i)}(\varepsilon_0) + 2\Delta^{(i)}} - \delta g_r^{(i)} \right) \mathrm{P}_i \,, \qquad (6)$$

where P_i is the probability to find the electron in the layers i (well or barrier). It is an expectation value of the bulk g factor calculated however with an (energy dependent) effective gap $\varepsilon_g^{(i)}(\varepsilon_0)$ ($= \varepsilon_0 - E_c^{(i)} + E_g^{(i)}$); this formula generalizes that of Roth et al. for the bulk [20] and is part of our analytical solution for the g-factor renormalization in 2D structures. It is particularly useful when the electron density of probability is concentrated in the active layers only, so that $g_\perp$ is determined by the confinement energy shift only, as already observed experimentally [36]. The known bulk formula is recovered in limits of $L_w \to 0$ and of sufficiently large L_w, when $\varepsilon_g^b(\varepsilon_0) \to E_g^b$ (with $P_w = 0$ and $P_b = 1$) and $\varepsilon_g^w(\varepsilon_0) \to E_g^w$ (with $P_w = 1$ and $P_b = 0$) respectively (note that the energy dependent effective mass also goes to the bulk band-edge effective mass, i.e. in these bulk limits one has respectively $m_b(\varepsilon_0) = m_b^*$ and $m_w(\varepsilon_0) = m_w^*$).

As a practical example let's consider $InP/InGaAs/InP/InGaAs/InP$ symmetric DQWs and $Insulator/InGaAs/InP/InGaAs/InP$ asymmetric DQWs structures, which depend on the same set of parameters, formed by the width of the $InGaAs$ and (middle) InP nanolayers, L_w and L_b, plus their bulk band parameters and band offset, and can then be better compared in order to assess the effects of SIA on this mesoscopic renormalization.

The recipe is then: for each point in the space spanned by the two varying parameters, L_w and L_b, we 1) solve the unperturbed problem to obtain ψ_0 and ε_0, the wavefunction and energy of the ground state of the Kane's DQW problem; then 2) calculate $z_0 = \langle z \rangle_{\psi_0}$ and the probabilities $P_i = \int_i |\psi_0|^2 dz$; and finally 3) substitute them into the equations above and get Δg^{DQW}, $g_\perp^{DQW}$ and $g_\parallel^{DQW}$.

With a color code, Figure 1 shows the obtained anisotropy maps for symmetric (a) and asymmetric (b) DQW structures, showing rich landscapes with qualitative differences, particularly in the strong coupling regime at the small L_b region. Note first that for the symmetric structures (SDQWs), the L_w-dependence of

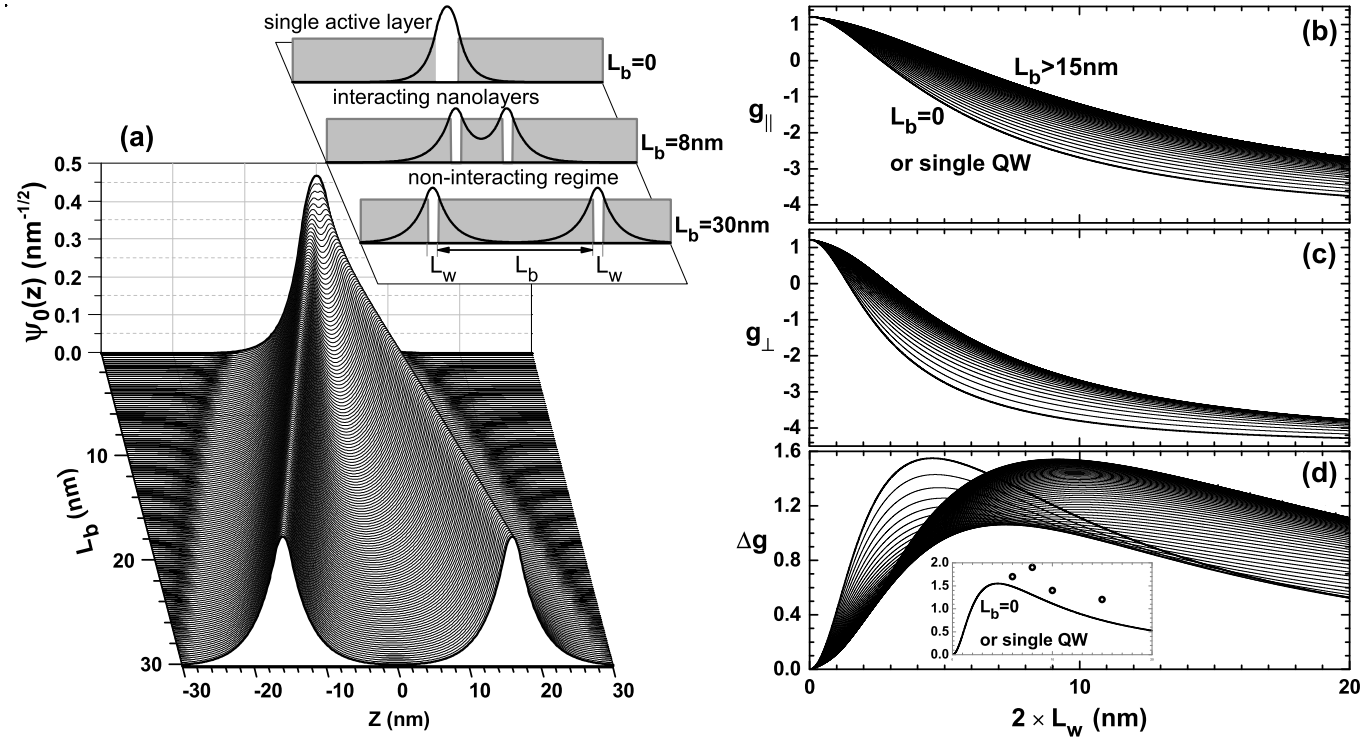

FIG. 2. Detailed results for the effective g factor of electrons in InGaAs/InP symmetric DQW structures, illustrated in the inset, with examples of the three different interacting regimes, corresponding to inter-well barrier width L_b zero, intermediate and sufficiently large; $L_w = 2\ nm$. Layers of InP and $In_{0.53}Ga_{0.47}As$ are considered with the following parameters: $E_g^{InP} = 1.424\ eV$, $\Delta_{so}^{InP} = 0.108\ eV$, $g^*_{InP} = 1.2$; and $E_g^{InGaAs} = 0.813\ eV$, $\Delta_{so}^{InGaAs} = 0.326\ eV$, $g^*_{InGaAs} = -4.5$ and $m^*_{InGaAs} = 0.041\ m_e$; [44] with a conduction-band offset of $0.25\ eV$ [45]. It is plotted: in (a) $\psi_0(z)$, and, as a function of L_w, $g_\perp$, $g_\parallel$ and Δg, in (b), (c) and (d), respectively. In (a), L_b varies from zero (on top) up to $30nm$ (bottom) in units of $0.2\ nm$, used also in the other plots. In (d) one sees the anisotropy Δg^{SDQW} interpolating from one single QW limit to another, as L_b goes from zero up to a sufficiently large value, as discussed in the text, and the inset shows the comparison with available experimental data [24].

the anisotropy for different values of L_b always satisfies the bulk conditions; i.e. independent of L_b, the g-factor anisotropy goes indeed to zero as $L_w \to 0$ or ∞, and that Δg presents always a single maximum, limited though by the maximum Δg^{QW}. By increasing the width of the InP barrier between the $InGaAs$ nanolayers, a continuous crossover from one non-interacting single QW limit to another is obtained (i.e., from a $2L_w$ wide QW to an L_w one); one exactly obtains $\Delta g^{SDQW}(L_w, L_b = 0) = \Delta g^{QW}(2L_w)$ and $\Delta g^{SDQW}(L_w, L_b \to \infty) = \Delta g^{QW}(L_w)$.

Probably the most interesting difference seen in asymmetric DQWs is the large negative anisotropies (down to $\Delta g = -2.4$) seen in the small area at the lower left angle of the map, corresponding to thin layer structures, just on the right of the black area, which is the region of the asymmetric structures with no allowed bound states. The differences in g-factor anisotropy between SDQWs and ADQWs are better understood with their corresponding explicit expressions. In flat-band structures, the expectation value in Eq. 5 is easily computed and Δg^{2D} is seen to be given in terms of the density of probability $\mathcal{P}$ ($= |\psi_0|^2$) at the different interfaces. In SDQWs there are only two non-equivalent interfaces, called 1 and 2, and one gets:

$$\Delta g^{SDQW} = \left[(\mathcal{P}_2 - \mathcal{P}_1)\, L_b + 2\mathcal{P}_2\, L_w \right] \frac{4m_0\, \delta\beta}{\hbar^2}, \qquad (7)$$

with the z-origin taken at the middle of the structure (see Fig.2), thus $z_0 = 0$, $\mathcal{P}_1 = |\psi_0(L_b/2)|^2$ and $\mathcal{P}_2 = |\psi_0(L_w + L_b/2)|^2$. In the ADQWs here considered, instead, with the z-origin taken at the leftmost infinite barrier with $|\psi_0(z=0)|^2 = 0$ (see Fig.3), three non-equivalent interfaces contribute (at $z = L_w, L_w + L_b, 2L_w + L_b$), and numbering them from the left one gets:

$$\Delta g^{ADQW} = \Big[(\mathcal{P}_3 - \mathcal{P}_2 + \mathcal{P}_1)\, (L_w - z_0) + (\mathcal{P}_3 - \mathcal{P}_2)\, L_b + \mathcal{P}_3 L_w \Big] \frac{4m_0\, \delta\beta}{\hbar^2}\,. \qquad (8)$$

These expressions complete the analytical solution and make clear each feature of the maps in Figure 1, with a look at the corresponding ψ_0, as well as at the individual elements $g_\perp$ and $g_\parallel$. See for instance the results in Figures 2 and 3 for $L_w = 2\,nm$ SDQWs and ADQWs respectively, with varying L_b in a fine grid ($0.2\,nm$), where (a) shows $\psi_0(z)$, (b) $g_\perp$, (c) $g_\parallel$ and (d) Δg, and the insets give examples of the three different interacting regimes,

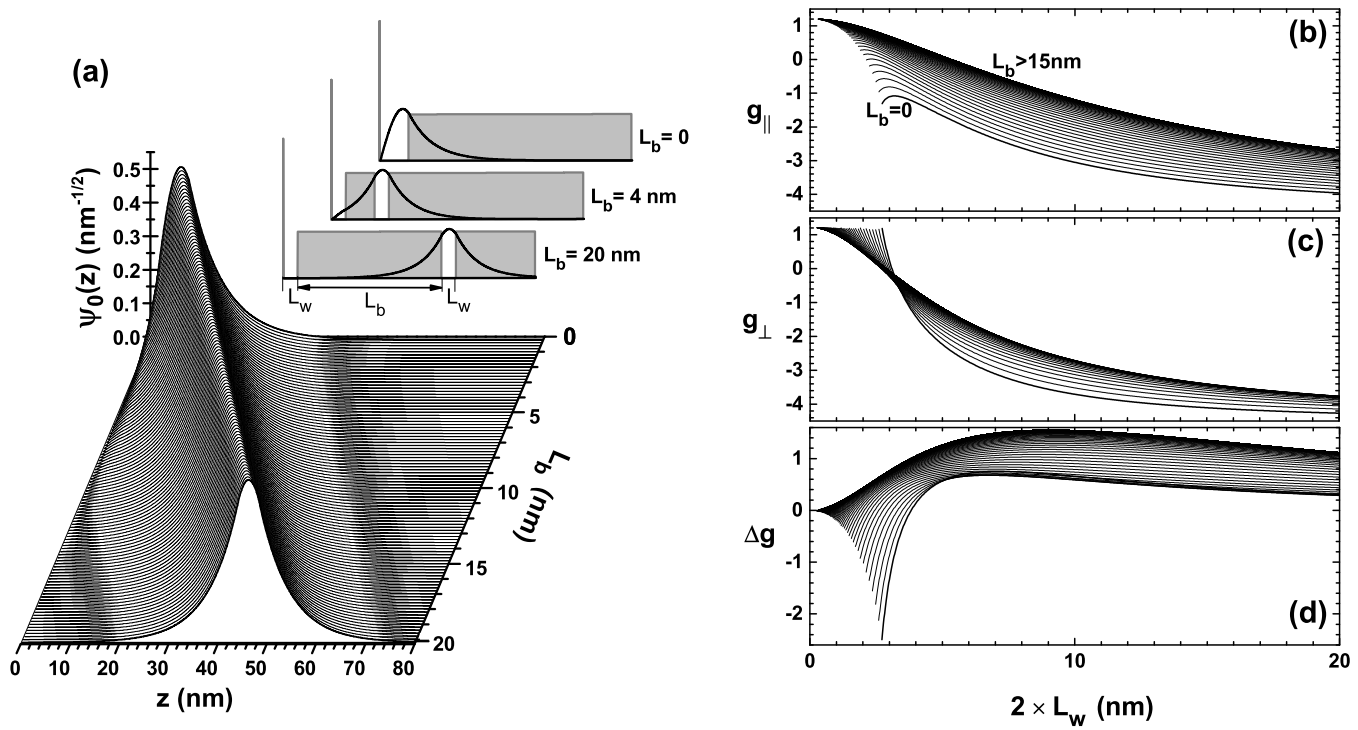

FIG. 3. Unperturbed wave-function and renormalized effective g factors for asymmetric DQW structures of the type $Insulator/InGaAs/InP/InGaAs/InP$, illustrated in the inset. L_w and L_b give the width of the InGaAs active layers and that of the tunneling InP barrier. The parameters used were as in Figure 2. The differences seen with respect to the SDQW results, derive from the SIA and are explained with the Rashba spin-orbit coupling in these structures (see the discussion in the text).

i.e. the non-interacting single QW, in the limits of $L_b = 0$ and $L_b >> L_w$, and the coupled regime in between.

The SDQW and ADQW ψ_0 are quite different; in ADQWs, $|\psi_0|^2$ is always concentrated in only one layer (that on the right, far from the large barrier on the left), while in SDQWs it splits equally between the two. To this corresponds an important qualitative difference also in z_0 as a function of L_w and L_b; while it is always zero in SDQWs, in ADQWs instead, it does vary significantly and is responsible for the negative anisotropies in very thin layer structures. In such thin layer limit, ψ_0 describes states with energy close to the top of the InP barrier, near the region with no allowed bound states, and feels strongly the asymmetry of the confining potential. For this reason the SDQW and ADQW results in this regime present larger contrast, and the ADQW z_0 is pushed away from the larger barrier, leading to the negative anisotropies.

Experimentally, the g-fator renormalization in InGaAs nanolayers has been investigated by Kowalski et al. [24], and more recently also by Herzog et al. [8]. Despite a sign controversy, the large confinement-induced anisotropy of the g factor in InGaAs QWs was confirmed in both studies. Modulation doping structures were used and a direct comparison with theory would require precise knowledge of the structure parameters and its self-consistent band-profile. Nevertheless, in the inset of Fig. 2 (d) we compare our flat-band results with plain data of Ref. [24] and obtain a reasonably good agreement, similarly to that already shown for GaAs systems [40]. Note that the curve in the inset is for symmetric QWs, which for this experimental L_w range, coincide with the results for the asymmetric QWs considered here. However, studies of samples with symmetric and asymmetric InGaAs DQW structures are still necessary in order to fully verify the above predictions for the large g-fator renormalization and anisotropy in these structures with interacting nanolayers.

Summarizing, we have solved the g-factor renormalization in III-V semiconductor DQW structures, within the multiband envelope function and perturbation approximations using the 8×8 Kane model for the bulk. Symmetric and asymmetric structures have been considered. Useful expressions are derived which explain well the available experimental data, and are applied to calculate the main effective g-factor components for electrons in $InP/InGaAs/InP/InGaAs/InP$ SDQWs and $Insulator/InGaAs/InP/InGaAs/InP$ ADQWs. With the resulting g-factor anisotropy as a function of the $InGaAs$-layer width and the middle InP-layer width, 2D maps were then constructed and compared to assess the effects of SIA on the g-factor mesoscopic renormal-

ization. The qualitative differences are simply explained with the structure's unperturbed wave-function ψ_0. Besides the specific numerical predictions for the $InGaAs$ DQW structures, the overall consistency of the results, shown over the whole space of the structure's parameters, and the general expressions derived give enough ground to believe that the present simple and transparent calculation can guide/help further research to fully understand the mesoscopic renormalization of the electron g factor in nanostructures.

Acknowledgments: EAAS is thankful to the Scuola Normale Superiore di Pisa, for the kind hospitality. Support from the brazilian agencies FAPESB, FAPESP (2016/03854-9), CAPES and CNPq is also acknowledged.

[1] G. Bastard, J. Brum, and R. Ferreira, in *Semiconductor Heterostructures and Nanostructures*, Solid State Physics, Vol. 44, edited by H. Ehrenreich and D. Turnbull (Academic Press, 1991) pp. 229 – 415.
[2] H. Kroemer, Rev. Mod. Phys. **73**, 783 (2001).
[3] M. Stern, V. Umansky, and I. Bar-Joseph, Science **343**, 55 (2014).
[4] S. S. Krishtopenko, W. Knap, and F. Teppe, Sci. Rep. **6**, 30755 (2016).
[5] X. G. Peralta, S. J. Allen, M. C. Wanke, N. E. Harff, J. A. Simmons, M. P. Lilly, J. L. Reno, P. J. Burke, and J. P. Eisenstein, Appl. Phys. Lett. **81**, 1627 (2002).
[6] I. Žutić, J. Fabian, and S. Das Sarma, Rev. Mod. Phys. **76**, 323 (2004).
[7] V. Mourik, K. Zuo, S. M. Frolov, S. R. Plissard, E. P. A. M. Bakkers, and L. P. Kouwenhoven, Science **336**, 1003 (2012).
[8] F. Herzog, H. Hardtdegen, T. Schäpers, D. Grundler, and M. A. Wilde, New J. Phys. **19**, 103012 (2017).
[9] A. Tadjine, Y.-M. Niquet, and C. Delerue, Phys. Rev. B **95**, 235437 (2017).
[10] F. Qu, J. van Veen, F. K. de Vries, A. J. A. Beukman, M. Wimmer, W. Yi, A. A. Kiselev, B.-M. Nguyen, M. Sokolich, M. J. Manfra, F. Nichele, C. M. Marcus, and L. P. Kouwenhoven, Nano Lett. **16**, 7509 (2016).
[11] X. Mu, G. Sullivan, and R.-R. Du, Appl. Phys. Lett. **108**, 012101 (2016).
[12] V. V. Belykh, D. R. Yakovlev, J. J. Schindler, E. A. Zhukov, M. A. Semina, M. Yacob, J. P. Reithmaier, M. Benyoucef, and M. Bayer, Phys. Rev. B **93**, 125302 (2016).
[13] M. A. T. Sandoval, E. A. de Andrada e Silva, A. F. da Silva, and G. C. L. Rocca, Semicond. Sci. Technol. **31**, 115008 (2016).
[14] M. Li, Z.-B. Feng, L. Fan, Y. Zhao, H. Han, and T. Feng, J. Magn. Magn. Mater. **403**, 81 (2016).
[15] M. Pakmehr, A. Khaetskii, B. D. McCombe, N. Bhandari, M. Cahay, O. Chiatti, S. F. Fischer, C. Heyn, and W. Hansen, Appl. Phys. Lett. **107** (2015).
[16] L.-W. Yang, Y.-C. Tsai, Y. Li, A. Higo, A. Murayama, S. Samukawa, and O. Voskoboynikov, Phys. Rev. B **92**, 245423 (2015).
[17] E. Ridolfi, E. A. de Andrada e Silva, and G. C. La Rocca, Phys. Rev. B **91**, 085313 (2015).
[18] A. V. Shchepetilnikov, Y. A. Nefyodov, I. V. Kukushkin, L. Tiemann, C. Reichl, W. Dietsche, and W. Wegscheider, Phys. Rev. B **92**, 161301 (2015).
[19] H. Kosaka, A. Kiselev, F. Baron, K. Wook Kim, and E. Yablonovitch, Electronic Letters **37**, 464 (2001).
[20] L. M. Roth, B. Lax, and S. Zwerdling, Phys. Rev. **114**, 90 (1959).
[21] T. P. Smith III and F. F. Fang, Phys. Rev. B **35**, 7729 (1987).
[22] E. L. Ivchenko and A. A. Kiselev, Sov. Phys. Semicond. **26**, 827 (1992).
[23] M. J. Snelling, G. P. Flinn, A. S. Plaut, R. T. Harley, A. C. Tropper, R. Eccleston, and C. C. Phillips, Phys. Rev. B **44**, 11345 (1991).
[24] B. Kowalski, P. Omling, B. K. Meyer, D. M. Hofmann, C. Wetzel, V. Härle, F. Scholz, and P. Sobkowicz, Phys. Rev. B **49**, 14786 (1994).
[25] R. Hannak, M. Oestreich, A. Heberle, W. Ruhle, and K. Kohler, Solid State Communications **93**, 313 (1995).
[26] P. Le Jeune, D. Robart, X. Marie, T. Amand, M. Brosseau, J. Barrau, and V. Kalevcih, Semicond. Sci. Technol. **12**, 380 (1997).
[27] E. Ivchenko, A. Kiselev, and M. Willander, Solid State Communications **102**, 375 (1997).
[28] Q. X. Zhao, M. Oestreich, and N. Magnea, Appl. Phys. Lett. **69**, 3704 (1996).
[29] A. A. Sirenko, T. Ruf, M. Cardona, D. R. Yakovlev, W. Ossau, A. Waag, and G. Landwehr, Phys. Rev. B **56**, 2114 (1997).
[30] A. A. Kiselev, E. L. Ivchenko, and U. Rössler, Phys. Rev. B **58**, 16353 (1998).
[31] A. A. Kiselev, K. W. Kim, and E. L. Ivchenko, physica status solidi (b) **215**, 235 (1999).
[32] A. Malinowski and R. T. Harley, Phys. Rev. B **62**, 2051 (2000).
[33] R. Kotlyar, T. L. Reinecke, M. Bayer, and A. Forchel, Phys. Rev. B **63**, 085310 (2001).
[34] X. C. Zhang, K. Ortner, A. Pfeuffer-Jeschke, C. R. Becker, and G. Landwehr, Phys. Rev. B **69**, 115340 (2004).
[35] M. de Dios-Leyva, E. Reyes-Gómez, C. A. Perdomo-Leiva, and L. E. Oliveira, Physical Review B **73**, 085316 (2006).
[36] I. A. Yugova, A. Greilich, D. R. Yakovlev, A. A. Kiselev, M. Bayer, V. V. Petrov, Y. K. Dolgikh, D. Reuter, and A. D. Wieck, Phys. Rev. B **75**, 245302 (2007).
[37] P. Pfeffer and W. Zawadzki, Phys. Rev. B **74**, 233303 (2006).
[38] S. Tomimoto, S. Nozawa, Y. Terai, S. Kuroda, K. Takita, and Y. Masumoto, Phys. Rev. B **81**, 125313 (2010).
[39] A. Bruno-Alfonso, F. E. López, N. Raigoza, and E. Reyes-Gómez, The European Physical Journal B **74**, 319 (2010).
[40] M. A. Toloza Sandoval, A. Ferreira da Silva, E. A. de Andrada e Silva, and G. C. La Rocca, Phys. Rev. B **86**, 195302 (2012).
[41] L. G. Gerchikov and A. V. Subashiev, Sov. Phys. Semicond. **26**, 73 (1992).
[42] E. A. de Andrada e Silva, G. C. La Rocca, and F. Bassani, Phys. Rev. B **50**, 8523 (1994).

[43] E. de Andrada e Silva, G. La Rocca, and F. Bassani, Phys. Rev. B **55**, 16293 (1997).
[44] in *Landolt-Bornstein New Series*, Vol. 3/22a, edited by O. Madelung (Springer, Berlin, 1987).
[45] J. Davies, *Physics of Low-dimensional Semiconductors: An Introduction* (Cambridge University Press, 1998).